applied optics

Improved algorithm for the transmittance estimation of spectra obtained with SOIR/Venus Express

LOIC TROMPET,[1,*] ARNAUD MAHIEUX,[1,2] BOJAN RISTIC,[1] SÉVERINE ROBERT,[1] VALÉRIE WILQUET,[1] IAN R. THOMAS,[1] ANN CARINE VANDAELE,[1] AND JEAN-LOUP BERTAUX[3]

[1]*Planetary Aeronomy, Royal Belgian Institute for Space Aeronomy, 3 Avenue Circulaire, 1180 Brussels, Belgium*
[2]*Fonds National de la Recherche Scientifique, Brussels, Belgium*
[3]*LATMOS/IPSL, Université Versailles St-Quentin, CNRS/INSU, 11 Boulevard d'Alembert, 78280 Guyancourt, France*
Corresponding author: loic.trompet@aeronomie.be

The Solar Occultation in the InfraRed (SOIR) instrument onboard the ESA Venus Express spacecraft, an infrared spectrometer sensitive from 2.2 to 4.3 μm, probed the atmosphere of Venus from June 2006 until December 2014. During this time, it performed more than 750 solar occultations of the Venus mesosphere and lower thermosphere. A new procedure has been developed for the estimation of the transmittance in order to decrease the number of rejected spectra, to check that the treated spectra are well calibrated, and to improve the quality of the calibrated spectra by reducing the noise and accurately normalizing it to the solar spectrum.   © 2016 Optical Society of America

1. INTRODUCTION

The SOIR (Solar Occultation in the InfraRed) spectrometer was part of the scientific payload onboard the Venus Express (VEx) orbiter of the European Space Agency (ESA) [1,2]. The SOIR instrument and its calibration have already been extensively described elsewhere [1,3–5], and only a summary will be given here. SOIR operated in the near infrared, being sensitive in the 2.2–4.3 μm (2200 to 4370 cm^{-1}) spectral range. It combined an echelle grating in front of which an acousto-optical tunable filter (AOTF) was placed for the selection of the spectral interval recorded. The spectral domain is divided in 94 regions corresponding to the diffraction orders of the echelle grating (101–194). During a solar occultation observation, SOIR was able to scan up to four orders, on a one second cycle basis. The SOIR detector has 320 pixel columns along the wavenumber axis and 256 pixels in the spatial direction, of which only 32 rows are illuminated. Telemetry limitations implied that only 8 rows of 320 pixels could be downlinked per second to Earth. For this reason, the pixel lines had to be binned onboard before being sent to Earth. Several binning schemes were used during the mission, varying the number of orders scanned and the number of binned pixel rows. They are summarized in Table 1. For most of the measurements, four orders were scanned. In the beginning of the mission, the rows were binned in 2 groups of 16 rows. After orbit

262, the rows were separated in 2 bins of 12 rows to avoid taking into account the side rows, which were less illuminated.

Most of the solar occultation observations were made using 2 bins of 12 rows, see Table 1. Measurements made using 4 bins of 3 rows and 8 bins of 3 rows have not been used for solar occultation observations but for other measurements dedicated to calibration [3].

A solar occultation observation consists of measuring the solar radiation passing through the atmosphere: during an orbit, an occultation occurs when the spacecraft passes behind the planet with respect to the Sun, entering the planet's shadow. Another occultation occurs when the spacecraft exits the shadow of the planet. These geometries are called ingress and egress, respectively. An egress is effectively identical to an ingress if reversed in time. During an ingress, the recording of spectra begins well before the line of sight of SOIR intersects the top layers of the atmosphere, which has arbitrarily been fixed at a 220 km altitude. The spectra taken above this altitude provide a reference for the calculation of the transmittances.

Individual spectra are grouped by bin and diffraction order for each observation: throughout SOIR's lifetime, 6232 of these sets of spectra were measured during 3219 orbits of Venus during over eight years of operation. SOIR made 1468 valid measurements from 12 May 2006 to 27 November 2014. Among

Table 1. List of Binning Options Used for SOIR during Solar Occultation Observations

Number of Scanned Order	Number of Binning Group	Number of Detector Lines in Each Bin	Number of Times Option was Used
4	2	16	46
		12	710
2	4	4	2
		3	0
1	8	4	21
		3	0

them, SOIR performed 779 solar occultation measurements of the Venusian atmosphere during its lifetime.

The spectral calibration [5,6], i.e., the relationship between pixel number and wavenumber for a given diffraction order, is obtained by comparing known solar lines to SOIR's spectra of the Sun outside of the atmosphere and made over the whole wavenumber range of the instrument. The complete procedure and determination of the spectral resolution are given in Vandaele *et al.* (2013) [6]. This paper provides all complementary information about the production of the calibrated data from the PSA level 2 data to the PSA level 3 data, i.e., the corrections related to the detector, the determination of the measurement altitudes, and a description of the archive's content.

The present work, which describes the procedure used to determine the transmittance spectra and their associated signal-to-noise ratio (SNR), is the follow-up of Vandaele *et al.* (2013).

Sounding atmospheres by occultation is widely used in space and Earth missions. Many of these instruments perform solar occultation, such as SAGE II [7], SAGE III [8], ACE-MAESTRO [9], and SCHIAMACHY [10]. Others use the stellar occultation technique, similar to solar occultation but made by pointing to a star other than the Sun (GOMOS [11], SPICAM [12], and SPICAV-UV [13]). The estimation of the transmittance from the data of these instruments is usually based on the determination of a reference Sun spectrum calculated as the average of several solar spectra recorded outside the atmosphere. This simple average seems to be sufficient to define the reference with enough accuracy for most of the instruments cited above. However, SOIR requires a more complex method for reasons described in Section 2.D.

2. CALCULATION OF THE TRANSMITTANCES

Prior to calculating transmittances, several corrections have to be applied to the raw spectra to obtain the PSA level 2 data (for more details, see Refs. [3,6]). First, the thermal and dark current are measured and subtracted onboard. Second, for low signal levels, we have to take into account the nonlinearity of the response of the detector. Other corrections, such as the pixel-to-pixel variability correction and the sensitivity correction, have been studied in detail in previous papers [3,4,6]. Since the transmittance calculation consists in calculating the ratio of two spectra obtained during the same observation, some of these corrections will cancel out.

In the next sections, we describe the new process used to compute the transmittances of the observation measurements. Then, the results of the new code (called v2.0) and comparisons with the old spectra are made and discussed.

A. Determination of the Measurement Altitude

The observation geometry of each measurement is calculated using SPICE kernels calculated by ESAC [14] and the SPICE toolkit provided by NAIF (Navigation and Ancillary Information Facility of NASA). Of importance to the calculation of the transmittance is the instantaneous tangent altitude, i.e., the lowest altitude reached by the line of sight during the record of one spectrum. A 10 arc min offset with respect to the center of the Sun was introduced to the inertial pointing to compensate for the atmospheric refraction. This has to be considered when determining the tangent altitude.
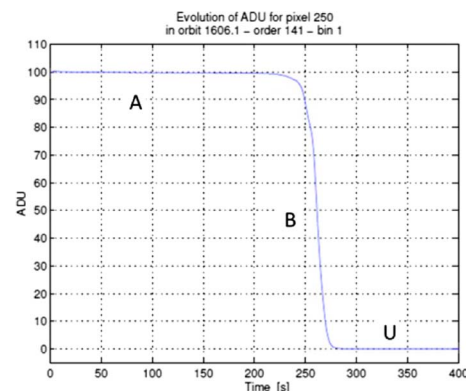
B. Description of the Algorithm Producing the Transmittances

Figure 1 shows an example of the signal in analog digital units (ADU) measured on one detector pixel during an ingress. Here, elapsed time after the record of the first spectrum is shown on the x-axis; however this could equally be tangent altitude or measurement index (i.e., spectrum number).

The signal in Fig. 1 can be separated into three parts:

• A, the "Sun region": the SOIR line of sight does not cross the atmosphere. This region extends above a tangent altitude of 220 km.

• B, the "penumbra region": the SOIR line of sight crosses Venus' atmosphere and the Sun's light is not totally absorbed by the atmosphere. This region extends from 60 to 220 km of tangent altitude and it is in this region where transmittances are calculated.

• U, the "umbra region": the SOIR line of sight still crosses the atmosphere of the planet but the Sun's light is totally absorbed. This region covers the tangent altitudes lower than 60 km.

The transmittances are obtained by applying the following procedure: the signal in the Sun region is fitted to a first-order polynomial with respect to the time of the measurement; we determine the extrapolation of that fit in the penumbra region; the transmittance is then obtained by dividing the value of the
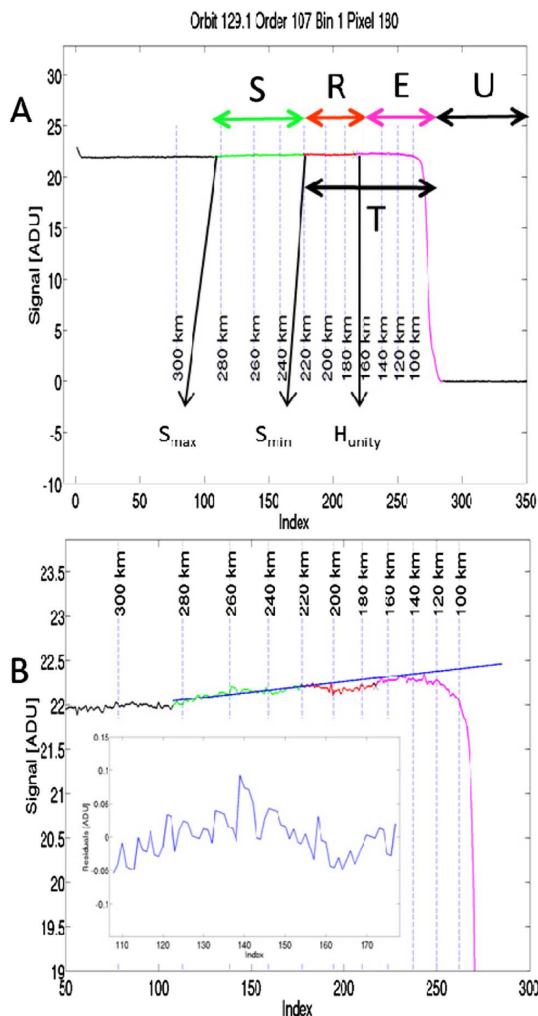

Fig. 1. Example of the signal obtained on one pixel during a solar occultation (ingress).

signal in the penumbra region by that extrapolation. This operation is done for each pixel independently.

At high altitude, for tangent altitudes larger than 180 km, the transmittance T should be around 1: $T - \delta T < 1 < T + \delta T$, where δT is the associated measurement error defined in [6]. If the Sun region signal does not show a linear behavior with the tangent altitude, the transmittances might not fulfill this condition. In such a case, a subregion is chosen and the regression calculation is made on this region instead.

Five criteria have been introduced, requiring the definition of several subregions within the Sun and penumbra regions, as shown in Fig. 2(A). For clarity, we have plotted the data for only one pixel in this figure. The black lines are the measured signal for the pixel considered. All subregions will be defined as follows:

• S is the region in the Sun region that is used to calculate the linear regression. The linear regression is plotted in green in Fig. 2(A).

• T is the whole subregion on which the transmittances are computed, i.e., the region between the last index of the S subregion and the tangent altitude of 60 km.

• H_{unity} is a single index corresponding to the closest tangent altitude to the *unity altitude*, i.e., the altitude below which atmospheric absorption is occurring; this altitude is wavenumber dependent.

• R is the subregion of T containing all spectra with tangent altitudes above (H_{unity}). The extrapolation of the S subregion in R is shown in red in Fig. 2(A). This subregion is called the *reference* subregion.

• E is the subregion of T containing the spectra where the tangent altitudes are under the *unity altitude*. The extrapolated S subregion in E is shown in purple in Fig. 2(A). This subregion is called the *effective* subregion as absorption occurs at these corresponding tangent altitudes.

• U is the umbra region defined above. It extends between the tangent altitude of 60 km and the lowest tangent altitude where a measurement was done.

Figure 2(B), the fit of the signal in the S region and its extrapolation in the T region are shown. The residuals of the fit to subregion S are shown in the lower left of Fig. 2(B). None of the absolute values reach 0.1 ADU, and the coefficient of correlation is 0.837.

C. Working Principle of the Algorithm Producing the Transmittances

We begin with the spectra already corrected for detector nonlinearity (see Ref. [3]), i.e., those corresponding to the PSA level 2 data. As a first step, the corresponding tangent altitudes for each measurement index are calculated using NAIF SPICE routines and kernels.

The maximum tangent altitude used for the regression is initially set to the highest tangent altitude, and the minimum tangent altitude is set to 220 km. Tangent altitudes below 60 km belong to the umbra part of the spectra.
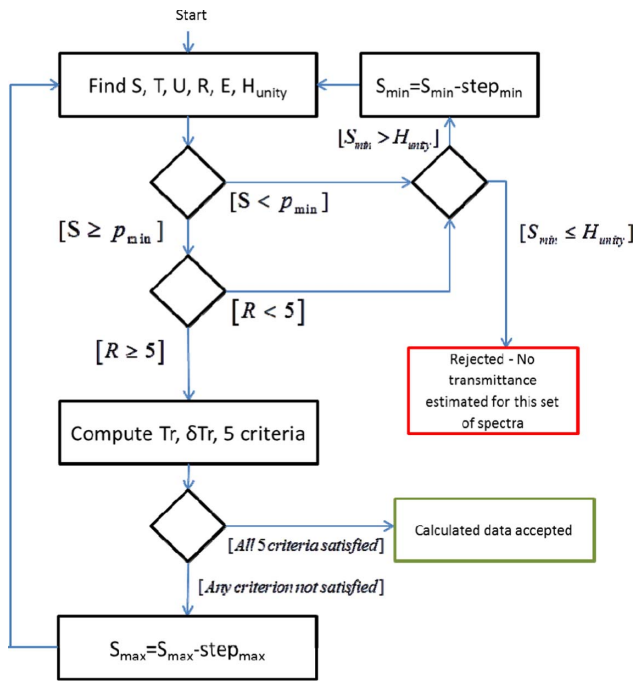
We perform a loop until an acceptable regression zone is found, i.e., until the condition: $Tr - \delta Tr < 1 < Tr + \delta Tr$ is satisfied. Figure 3 gives the flow chart of the different tests and computations done inside this loop.

In this flow chart, the variables S_{max} and S_{min} define the limits of the S region. The S region is expected to contain at least 20 indices. Thus, the parameter p_{min} is set to 20. The other parameters $step_{max}$ and $step_{min}$ are set to 10 (i.e., steps of 10 indices are performed) or one if the complete Sun region A contains only a few tens of indices. In the algorithm, the length of the R region is also checked: it has to contain more than four indices to have a good estimate of the fulfillment of the third criteria.

For each order, a minimum tangent altitude H_{unity} is defined for the linear regression calculation. This limit to the minimum altitude of the S region (S_{min}) has to be set since absorption lines might be present at lower altitudes. These have been defined knowing the highest altitude at which molecular species may be found in each order and are shown in Table 2.

The T region can thus be different from the B region defined in Fig. 1 since a part of T (the R region) can be used for the S region if necessary.

The transmittance $Tr(t)$ is calculated for each pixel and index of the defined penumbra region by dividing the values in

Fig. 2. (A) Separation of the Sun region in different zones for one detector pixel as a function of the index, i.e., the time after the beginning of the measurement. Lines corresponding to specific tangent altitudes are plotted. (B) Plot of the fit over the S region and extrapolation in the T region. The graph inside is the residuals of the fit.

Fig. 3. Flow chart of the code producing the transmittance calibrated spectra.

Table 2. Unity Altitude (H_{unity}) for Each Order[a]

Tangent Altitudes (km)	120	130	140	150	160	170
Orders	108	114	111	190	156	101
	109	115	112	191	157	102
	110	116	113		158	103
	134	117	128			104
	135	118	129			105
	136	119	130			106
	137	120	131			107
	138	121	132			159
	139	122	133			160
	140	123	148			161
	176	124	149			162
	177	125	150			163
	178	126	151			164
	179	127	155			165
	180	141	168			166
	181	142	169			167
	182	143	189			
	183	144	192			
	184	145	193			
	185	146	194			
	186	147				
	152					
	153					
	154					
	170					
	171					
	172					
	173					
	174					
	175					
	187					
	188					

[a]Above these values, no absorption can be present in the spectra.

the penumbra region $P(t)$ by the extrapolation of the linear regression performed over the values of the indices of the Sun region $S(t)$ (i.e., $\mathrm{Tr}(t) = P(t)/S(t)$). The noises in the Sun and umbra regions (δS and δU) are calculated as the standard deviation of the signal with time. δS contains all noise sources (photon noise, electronic noise, etc.), and δU can be considered as only composed of electronic noise. The noise in the penumbra region δP contains the electronic noise and a photon noise directly dependent on the signal.

The noise in the penumbra region δP, the noise $\delta \mathrm{Tr}(t)$ on the transmittance spectrum, and the SNR are obtained using equations in Eq. (2) of [6]. Some of them are recalled here in Eq. (1) as

$$\delta P(t) = \delta U + \sqrt{\mathrm{Tr}(t)}(\delta S - \delta U),$$
$$\delta \mathrm{Tr}(t) = \sqrt{\delta P(t)^2 + \mathrm{Tr}(t)^2 \delta S^2},$$
$$\mathrm{SNR}(t) = \frac{\mathrm{Tr}(t)}{\delta \mathrm{Tr}(t)}. \tag{1}$$

It may occur that the values of S do not change along the occultation. Then δS is close to zero and the SNR will have values artificially high for some pixels, which are flagged as *bad pixels*. To avoid this, these pixels are not considered in the criteria described hereafter. The transmittances and noises of the *bad pixels* are calculated at the end of the procedure using the values of their nearest neighbors.

Once the transmittance $\mathrm{Tr}(t)$ and the noise $\delta \mathrm{Tr}(t)$ have been computed, the criteria used to determine if the regression zone is valid can be applied. A criterion is considered as satisfied if it is fulfilled by 80% of the pixels. They are defined over the different regions as [see Eqs. (2)–(6)]

$$|1 - \mathrm{Tr}(i)| < f * \delta\mathrm{Tr}(i) \qquad i \in R, \tag{2}$$

$$\delta\mathrm{Tr}(i) < \frac{1}{\mathrm{SNR}_{min}} \qquad i \in R, \tag{3}$$

$$\delta\mathrm{Tr}(i) < f * \mathrm{std}(\mathrm{Tr}(R)) \qquad i \in R, \tag{4}$$

$$\mathrm{Tr}(i) - 1 < f * \delta\mathrm{Tr}(i) \qquad i \in E, \tag{5}$$

$$|1 - \mathrm{Tr}(H_{unity})| < f * \delta\mathrm{Tr}(H_{unity}), \tag{6}$$
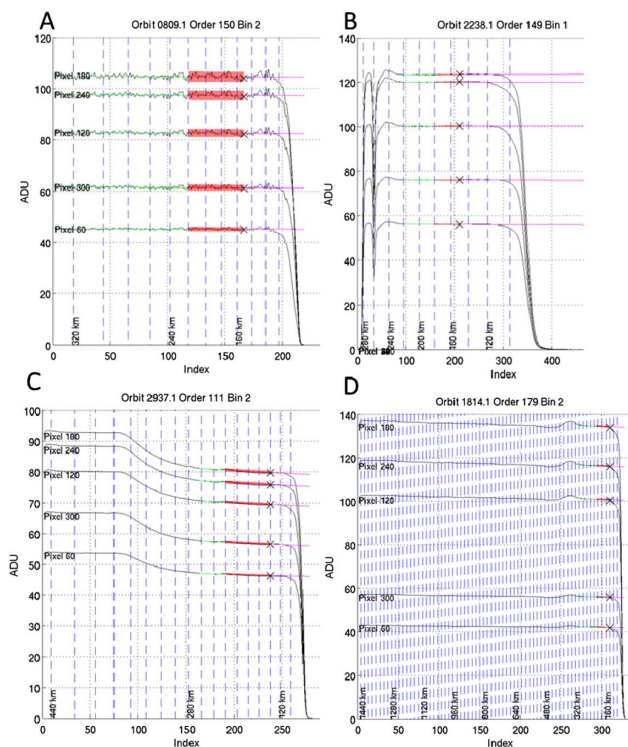
where SNR_{min} in Eq. (3) is a parameter that represents the minimum signal-to-noise ratio that we require from the transmittances (the default value is set to 200). f is a factor most of the time set to 2, but for few particularly noisy spectra, a value of 3 has been used. Equation (2) means that the estimated transmittance is required to have values that do not exceed $1 - 2 * \delta\mathrm{Tr}$ to $1 + 2 * \delta\mathrm{Tr}$. The three last criteria should logically always be fulfilled. They are useful to reject a very particular set of spectra. For example, we can see the importance of Eq. (5) in the case of Fig. 5.
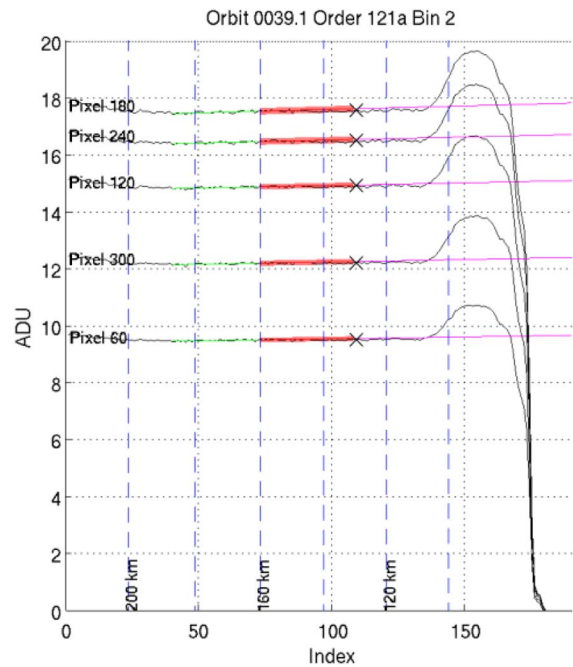
D. Examples

The signal is not always as ideal as the one in Fig. 2. Some particular cases are illustrated in Fig. 4 where the region of the linear regression is more complicated to find. The spectra of orbit 809.1 order 150 bin 2 [Fig. 4(A)] are more noisy. For orbit 2238.1 [Fig. 4(B)], the full Sun signal shows what seems like an off-pointing of the instrument and the algorithm found a linear regression region after this off-pointing. Orbit 2937.1 [Fig. 4(C)] also presents some off-pointing. A slightly non-constant signal can be seen at the end of the full Sun zone for orbit 1814.1 [Fig. 4(D)]. The linear regression region is defined after this bump.

For a few sets of spectra, the signal has a particular shape preventing production of calibrated spectra. An example of a set of spectra rejected by the new algorithm is presented in Fig. 5 (orbit 39.1). For each pixel, the signal shows a large increase after the unity altitude, so the fourth criterion will never be met [see Eq. (5)]: the transmittances in the penumbra region would be much larger than 1.

Figure 6 shows an example of estimated transmittances for the highest tangent altitude for the set of spectra corresponding to orbit 892.1 order 119 bin 1 (all spectra corresponding to different tangent altitudes are plotted on the same graph). These spectra have a regular pattern as they are mainly composed of lines of CO_2. The lines are spectrally resolved thanks to the high resolution of SOIR. The new spectra, which are above the unity altitude, have a mean value of 0.99851. The highest calculated transmittances with the old version 1.0 of the code [Fig. 6(A)]

Fig. 5. Example of a rejected set of spectra, with the index as a function of ADU. The black line is the signal, the green line is the fit in the S region, the red line is the R region, the purple line is the extrapolation in the E region, and the cross is the *unity altitude*.

have a mean value for all the spectra above the unity altitude of 1.00316. Thus, the new spectra are on average closer and smaller than 1.
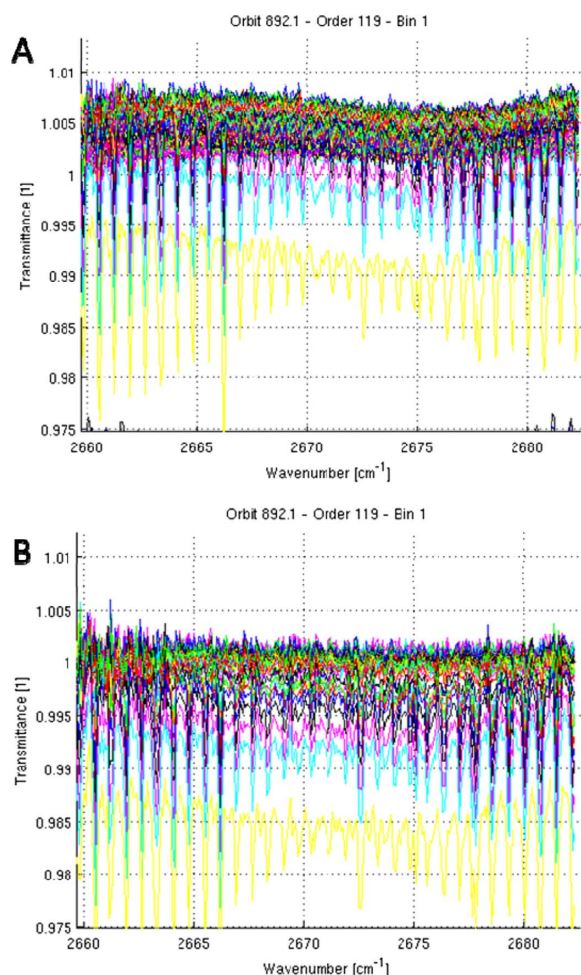
E. Statistics

The spectra obtained by the old and the new versions are compared in this section. The whole set of spectra cannot be used for this comparison for the following reasons.

The dataset obtained with the first version (v1.0) of the transmittance calculation code considered only orbits 1 to 2855.2. Some spectra could not be treated with the new code (v2.0) while some others were not treated by the old one. For consistency, comparisons are made on spectra present in both versions.

In addition, some other orbits have to be removed from the set of comparative orbits. Indeed, some noise values δT calculated with version 1.0 routines seem to be underestimated by a significant amount and behave linearly with time. This is not an expected behavior and clearly indicates a problem in the previous method. The noise values obtained for all orbits with the new version 2.0 and for some orbits with the old code v1.0 (orbit 341.1 and from orbits 2463.1 until 2855.2) are proportional to the signal. This seems logical as the noise depends on the signal; see Eq. (1). Thus, the noise calculated with v1.0 can be of two types: correct for orbits after orbit 2463 and incorrect for orbits before orbit 2463, except orbit 341.1. The noises calculated with v2.0 is correct for the whole set of observations.

Figures 7(A) and 7(B) show the noise for a complete set of pixels for one occultation, calculated using both the old code and new code, respectively. Passing along the direction of the pixels, we can see in Fig. 7(A) that the highest errors arise for

Fig. 4. Some examples of linear regression for different shapes for the full Sun zone for five pixels. The black line is the signal, the green line is the fit in the S region, the red line is the R region, the purple line is the extrapolation in the E region, and the cross is the *unity altitude*.
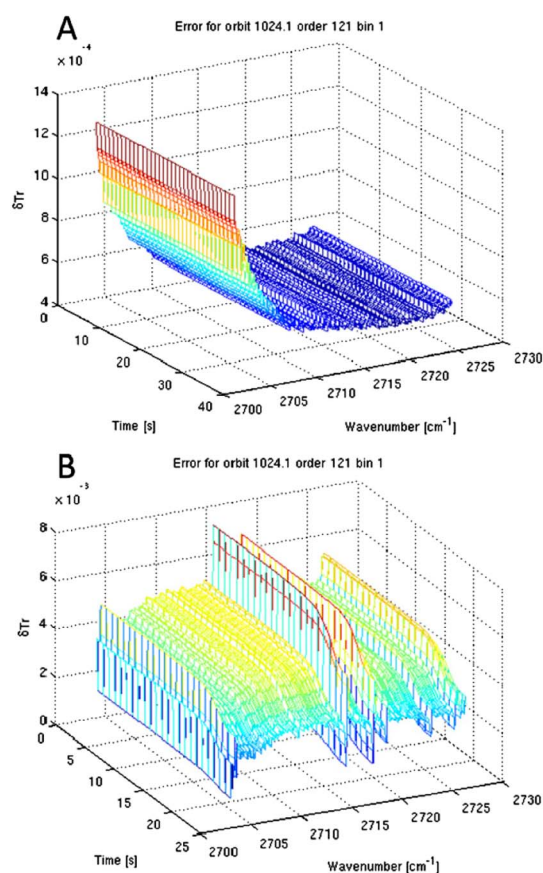
Fig. 6. Transmittances calculated by (A) version 1.0 and (B) version 2.0 for orbit 892.1 order 119 bin 1. The different spectra corresponding to different tangent altitudes are plotted on the same graph.

Fig. 7. Errors for orbit 1024.1, order 121 bin 1. (A) The old version is on top, and (B) the new version below (the scale of δT is in 10^{-4} for the old version and in 10^{-3} for the new one).

the first pixels. The error decreases over the 70 first pixels and the error is more constant for the next 250 next pixels. Figure 7(B) shows an error that has the shape of the related transmittance.

In the previous dataset, the bad pixels were not handled. A total of 52 sets of spectra containing such bad pixels have been identified using version 2.0 of the code.

To be sure to compare similar sets of spectra, any set of spectra produced with the previous version 1.0 and containing at least one of the cases above (calculated error with line shape or bad pixel) were not taken into account in the comparison. This strongly reduces the number of sets valid for the comparison, i.e., only 920 sets of spectra are left.

Table 3 lists several parameters that are used to make the comparison between the two versions of the code. The values in the second column (for the 920 suited sets of spectra) are of the order of magnitude of the values in the third column (for the whole 5921 sets of spectra) produced with v2.0. For the dataset used for the comparison, the new version produces mean transmittances closer to 1. The mean noise value is five times smaller for the new code, remembering that the

calculated errors by the previous version of the code 1.0 with the line shape and an order of magnitude lower than the new ones are not part of the 920 sets of spectra used for comparison. The new set of data contains also more indices above the absorption region. This means that transmittances are now obtained for higher altitudes. The mean noise value for the whole new dataset is moreover a third smaller than the one calculated for the comparison set.

The $T - 1 > 2\delta T$ comparison is larger for the new set of spectra because the noise is larger in the old dataset while the transmittances for both old and new versions are very similar. This can explain the "anticorrelation" observed between the noise and the success of the relation $T - 1 > 2\delta T$ in the two first columns.

The version 2.0 of the code has been used to determine the transmittances of 5921 sets of spectra over the 6232 total sets of spectra, i.e., 95% of the sets of spectra are present in PSA level 3. The main reason why the remaining sets of spectra could not be treated is that the Sun A region has an unsuitable shape (Fig. 5 is an example). In total, the new version contains 735 sets of spectra that were not present in the old version (among them, 271 sets of spectra before orbit 2855.2, i.e., the last calculated one with the old version of the code).

Table 3. Comparison of the Transmittances from Versions 1.0 (First Column) and 2.0 (Second Column)[a]

	Old (920 Sets of Spectra)	New (920 Sets of Spectra)	New (5921 Sets of Spectra)
Mean value of the signal of each pixel	0.996971	0.99744	0.996863
Standard deviation of the signal of each pixel	0.00542177	0.00528519	0.00773209
Mean of the noise	0.0161901	0.00300478	0.00250643
Maximum value of the noise	0.0252719	0.0108349	0.010403
Number of index contained in S	30.1609	48.1065	73.8787
Ratio of pixels over the whole indices that satisfies the relation $T - 1 > 2\delta T$	0.00362668	0.0177389	0.0232391

[a]The third column refers to the whole new dataset produced with v2.0.

3. CONCLUSIONS

The new version of the code used to produce the 0.3 internal level data for SOIR uses the formula from Vandaele *et al.* (2013) to compute the transmittances and their associated noise. As explained in the present paper, the transmittances are calculated by dividing the signal in the penumbra region by an extrapolated reference calculated from a linear regression in the full Sun region. In addition, five criteria have been defined to find the best regression region in the full Sun region to ensure reliable transmittance calculations.

An explanation of the code and some examples of accepted and rejected sets of spectra are given to help comprehension for future users.

Comparisons between some data obtained using the new and old versions of the code are given. The new version could manage more sets of spectra than the previous one. We show that the new version of the code produces reliable transmittances and errors.

REFERENCES

1. D. Nevejans, E. Neefs, E. Van Ransbeeck, S. Berkenbosch, R. Clairquin, L. De Vos, W. Moelans, S. Glorieux, A. Baeke, O. Korablev, I. Vinogradov, Y. Kalinnikov, B. Bach, J.-P. Dubois, and E. Villard, "Compact high-resolution space-borne echelle grating spectrometer with AOTF based on order sorting for the infrared domain from 2.2 to 4.3 micrometer," Appl. Opt. **45**, 5191–5206 (2006).
2. H. Svedhem, D. Titov, F. Taylor, and O. Witasse, "Venus Express mission," J. Geophys. Res. **114**, 3–21 (2009).
3. A. Mahieux, S. Berkenbosch, R. Clairquin, D. Fussen, N. Mateshvili, E. Neefs, D. Nevejans, B. Ristic, A. C. Vandaele, V. Wilquet, D. Belyaev, A. Fedorova, O. Korablev, E. Villard, F. Montmessin, and J.-L. Bertaux, "In-flight performance and calibration of SPICAV/ SOIR on-board Venus Express," Appl. Opt. **47**, 2252–2265 (2008).
4. A. Mahieux, V. Wilquet, R. Drummond, D. Belyaev, A. Federova, and A. C. Vandaele, "A new method for determining the transfer function of an acousto optical tunable filter," Opt. Express **17**, 2005–2014 (2009).
5. A. Mahieux, "Inversion of the infrared spectra recorded by the SOIR instrument on board Venus Express," Ph.D. dissertation (Université Libre de Bruxelles, 2011).
6. A. C. Vandaele, A. Mahieux, S. Robert, S. Berkenbosch, R. Clairquin, R. Drummond, V. Letocart, E. Neefs, B. Ristic, V. Wilquet, F. Colomer, D. Belyaev, and J.-L. Bertaux, "Improved calibration of SOIR/Venus Express spectra," Opt. Express **21**, 21148–21161 (2013).
7. W. P. Chu, M. P. McCormick, J. Lenoble, C. Brogniez, and P. Pruvost, "SAGE II inversion algorithm," J. Geophys. Res. **94**, 8339–8351 (1989).
8. L. E. Mauldin, R. Salikhov, S. Habib, A. Vladimirov, D. Carraway, G. Petrenko, and J. Comella, "Meteor-3M-/stratospheric aerosol and gas experiment III (SAGE III)," Proc. SPIE **3501**, 355–365 (1998).
9. C. T. McElroy, C. R. Nowlan, J. R. Drummond, P. F. Bernath, D. V. Barton, D. G. Dufour, C. Midwinter, R. B. Hall, A. Ogyu, A. Ullberg, D. I. Wardle, J. Kar, J. Zou, F. Nichitiu, C. D. Boone, K. A. Walker, and N. Rowlands, "The ACE-MAESTRO instrument on SCISAT: description, performance, and preliminary results," Appl. Opt. **46**, 4341–4356 (2007).
10. G. Lichtenberg, Q. Kleipool, J. M. Krijger, G. van Soest, R. van Hees, L. G. Tilstra, J. R. Acarreta, I. Aben, B. Ahlers, H. Bovensmann, K. Chance, A. M. S. Gloudemans, R. W. M. Hoogeveen, R. T. N. Jongma, S. Noël, A. Piters, H. Schrijver, C. Schrijvers, C. E. Sioris, J. Skupin, S. Slijkhuis, P. Stammes, and M. Wuttke, "SCIAMACHY level 1 data: calibration concept and in-flight calibration," in *Atmospheric Chemistry and Physics* (European Geosciences Union, 2006), Vol. **6**, pp. 5347–5367.
11. J.-L. Bertaux, E. Kyrölä, D. Fussen, A. Hauchecorne, F. Dalaudier, V. Sofieva, J. Tamminen, F. Vanhellemont, O. Fanton d'Andon, G. Barrot, A. Mangin, L. Blanot, J.-C. Lebrun, K. Pérot, T. Fehr, L. Saavedra, G. W. Leppelmeier, and R. Fraisse, "Global ozone monitoring by occultation of stars: an overview of GOMOS measurements on ENVISAT," in *Atmospheric Chemistry and Physics* (European Geosciences Union, 2010), Vol. **10**, pp. 12091–121480.
12. S. Lebonnois, E. Quémerais, F. Montmessin, F. Lefèvre, S. Perrier, J.-L. Bertaux, and F. Forget, "Vertical distribution of ozone on Mars as measured by SPICAM/Mars Express using stellar occultations," J. Geophys. Res. **111**, E09S05 (2006).
13. E. Quémerais, J.-L. Bertaux, O. Korablev, E. Dimarellis, C. Cot, B. R. Sandel, and D. Fussen, "Stellar occultations observed by SPICAM on Mars Express," J. Geophys. Res. **111**, E09S04 (2006).
14. C. H. Acton, "Ancillary data services of NASA's navigational and ancillary information facility," Planet. Space Sci. **44**, 65–70 (1996).